Optimal Data Transfer of SEH-WSN Node via MDP Based on Duty Cycle and Battery Energy

KANOK CHAROENCHAIPRAKIT[1], (Member, IEEE), **WEKIN PIYARAT**[1], (Member, IEEE), **AND KAMPOL WORADIT**[2], (Member, IEEE)

[1]Department of Electrical Engineering, Srinakharinwirot University, Ongkharak Campus, Bangkok 26120, Thailand
[2]OASYS Laboratory, Department of Computer Engineering, Chiang Mai University, Chiang Mai 50200, Thailand

Corresponding author: Wekin Piyarat (wekin@g.swu.ac.th)

ABSTRACT Applications in wireless sensor networks (WSNs) are rapidly spreading out over the world. The one critical point of WSNs is energy consumption, where the transmitted data is limited by battery energy. Solar energy is used to handle the depletion of the battery energy via photo voltaic (PV) panels. A solar energy harvesting WSN (SEH-WSN) node utilizes exponential decision-dynamic duty cycle scheduling based on prospective increase in energy (ED-DSP) to save battery energy by adjusting the duty cycle from an exponential curve and future solar energy. To estimate the prospective solar energy, a prediction technique is applied, but does not guarantee 100% accuracy. Hence, this paper proposes a Markov Decision Process (MDP) to schedule a duty cycle of an SEH-WSN node instead of the ED-DSP depending on the predicted energy. We evaluate its performance via MATLAB simulations with simple irradiance models and real annual irradiance data. The results show that the MDP policy outperforms the ED-DSP.

INDEX TERMS Solar energy harvesting, Markov decision process, wireless sensor network.

I. INTRODUCTION

Currently, many fields have seen a dramatic increase in sensor applications, especially in healthcare, agriculture, environmental monitoring and forecasting, transportation, security, and disaster management. These sensors are connected to various technologies such as the Internet of Thing (IoT), cloud computing, nanotechnology, and big data. In the future, many of these technologies may be integrated into networks and be run and maintained by applications [1].

Modern life and work are replete with IoT. The architecture of the IoT is essentially based on data links and interfaces to make things connectable and smart. Nevertheless, in this arrangement, a key factor remains energy consumption [2]. In big data, a large number of sensors, both mobile and stationary WSN nodes, are deployed in the environment. The Quality of Service (QoS) and a lifetime of WSNs can be improved with a well-designed system [3]. Due to the limitations of the WSN node battery capacity, an energy-aware adaptive sensing technique can be applied to calculate the sustainable sensing period based on residual battery energy that yields an optimal data gathering process [4].

The associate editor coordinating the review of this manuscript and approving it for publication was Jose Saldana.

Besides the energy consumption management within the WSN infrastructure, energy harvesting is another solution that is being continuously researched.

The energy harvesting technique utilizes ambient energy, such as solar, vibration, thermometric, wind flow, magnetic field, and acoustic noise, which can be converted to electricity. These energies can be applied to WSNs, where these become energy harvesting WSNs (EH-WSNs). Of all the methods currently available, solar energy has the highest potential in terms of harvesting energy $(mW/cm^3)(\mu W/cm^3)$ [5]. Hence, this article will only focus on an SEH-WSN scheme.

In addition, Medium Access Control (MAC) protocol can cause huge energy consumption in WSNs because of data collision and idle listening. A duty-cycle MAC protocol is initially used for non-rechargeable WSN nodes. If the MAC protocol operates in the high duty cycle, the active time is longer and more energy is consumed. Hence, the key to saving energy is to reduce idle listening periods by switching to sleep mode, which decreases wasted energy by up to 50% [6]. To deal with the issue of fluctuations in solar energy during the daytime, the duty cycle has to be adjusted to correspond to the strength of solar irradiance to yield the proper data transfer and prevent battery depletion.

With this concept, Exponential decision MAC (ED-MAC) protocols are proposed. These protocols performed with better results in a high packet delivery ratio and low energy consumption when compared to a receive initiated MAC (RI-MAC) protocol that is normally used in the general WSNs [7]. However, the ED-MAC protocols are the deterministic solution for the SEH-WSNs, which causes difficulties in guaranteeing optimal results.

This article proposes a stochastic approach with MDP, based on battery energy and a duty cycle of an SEH-WSN node to provide a duty cycle that maximizes the data transfer while preventing premature battery depletion.

The article is organized as follows: Section II describes the background and related works, including notations. Section III proposes a designed model. Section IV presents the proposed method in detail. Section V assesses the system performance with MATLAB simulations. Section VI discusses the evaluated results. Finally, Section VII states the conclusion of this article.

II. BACKGROUND AND RELATED WORKS
This section will provide the notations used in this article, followed by a presentation of the background and related works on MAC protocols for EH-WSNs, SEH-WSN nodes, solar irradiance and solar charging models, and an MDP. These subjects will initiate knowledge of our proposed method.

A. NOTATIONS
Script uppercase letters are denoted assets. For example, a set can be written as $\mathscr{A}$. Bold lowercase and uppercase letters are denoted as vectors and matrices. For example, a vector and matrix can be written as $\mathbf{a}$ or $\mathbf{A}$. Italic lowercase and uppercase letters are denoted as scalars. For example, a scalar can be written as a or A. Table 1 indicates the symbols and their definitions used in this article. For probability representation, the letter P with curly brackets as $P\{event\}$ is applied.

B. MAC PROTOCOLS FOR EH-WSNs
MAC protocol is considered to be a layer in the communication architecture for WSNs. Its function is to control the WSN node in transmitting signals through the air. The MAC protocol yields high throughput and fairness, but also less energy consumption and latency.

WSN nodes are usually deployed in the environment without access to a public power supply. Thus, a battery of the WSN node has to be replaced to prolong the network. To reduce energy consumption, a sensor MAC (S-MAC) protocol is used instead of a conventional wireless MAC protocol, such as IEEE 802.11 that delivers a high data transfer rate, but consumes a lot of energy [8].

The S-MAC protocol controls data accessing the medium by a contention-based technique with duty-cycle operation. One cycle consists of an active period and a sleep period. The sleep mode is used instead of an idle listening

TABLE 1. Symbols and descriptions.

Symbol	Description [Unit]
$\mathscr{A}$	Set of actions
$\mathscr{B}$	Set of battery energy levels
$\mathscr{D}$	Set of duty cycle levels
$\mathscr{G}$	Set of days that MDP policy transfers more data than ED-DSP
$\mathscr{Q}$	Set of days that ED-DSP transfers more data than MDP policy
$\mathscr{S}$	Set of States
$\mathbf{T}_D$	Matrix of duty cycle transition probability
$\mathbf{T}_B$	Matrix of battery energy transition probability
$\mathbf{T}_P$	Matrix of transition probability
$\mathbf{P}_{out}$	Vector of output energy at PV panel
$\mathbf{P}_p$	Vector of potentially charged energy probability
$\mathbf{R}$	Vector of reward
A_s	Area of a PV panel [m^2]
B	Battery energy [J]
B_c	Critical battery energy [J]
B_{th}	Threshold battery energy [J]
B_{max}	Maximum battery energy [J]
B_r	Residual battery energy [J]
D	Duty cycle [%]
D_c	Critical duty cycle [%]
D_{ED-DSP}	Duty cycle of ED-DSP protocol [%]
D_{ED-DSR}	Duty cycle of ED-DSR protocol [%]
D_{max}	Maximum duty cycle of ED-MAC protocol [%]
D_{min}	Minimum duty cycle of ED-MAC protocol [%]
D_{th}	Threshold duty cycle [%]
D_{tr}	Data transfer rate [bit/s]
C	Cost function
E_{charge}	Potentially charged energy in battery [J]
E_{cons}	Energy consumption in one duty cycle level [J]
E_e	Expected energy from solar energy harvesting [J]
E_{sur}	Surplus energy from a PV panel [J]
F	Cloudy sky factor
P	Transition probability
P_{charge}	Potentially charged power in battery [W]
P_{cons}	Power consumption during operation [W]
P_{out}	Output power at PV panel [W]
P_p	Potentially charged energy probability
I	Solar irradiance [W/m^2]
I_{clear}	Solar irradiance with clear sky [W/m^2]
I_{cloudy}	Solar irradiance with cloudy sky [W/m^2]
I_{max}	Maximum solar irradiance [W/m^2]
$I_{ETI_{max}}$	Maximum extraterrestrial irradiance [W/m^2]
T	Time period
T_{act}	Active time period
T_{duty}	Time period of duty cycle
T_{opt}	Operation time period
T_{tr}	Time that data transferred
a	Action member in action set
b	Battery member in battery set
d	Duty cycle member in duty cycle set
$a_1, a_2, b_1, b_2, c_1, c_2$	Cloudy sky model parameters
g	Day that MDP policy transfers more data than ED-DSP
q	Day that ED-DSP transfers more data than MDP policy
i,j,k,l,m,n,v,z	Index of vector, matrix or set
s	State member in state set
t	Time [h]
t_{rise}	Sunrise time [h]
t_{set}	Sunset time [h]
Δ	Different amount of data transfer [bit]
α	ED-MAC protocol constant
β	Charging controller efficiency [%]
η	PV panel efficiency [%]
γ	ED-MAC protocol variable
ϕ	Decision variable or randomized policy
ϕ^*	Optimal randomized policy
π^*	Optimal policy

mode due to the low amount of data transferred in WSN applications. Therefore, the WSN node can reduce energy consumption.
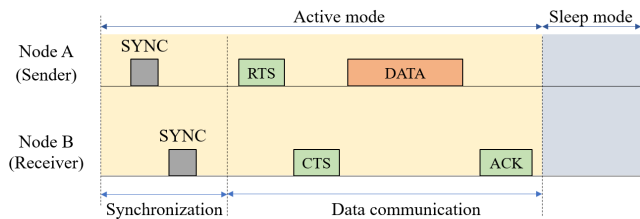
FIGURE 1. A scenario of sending the message from node A to node B in one duty cycle by using the S-MAC protocol.
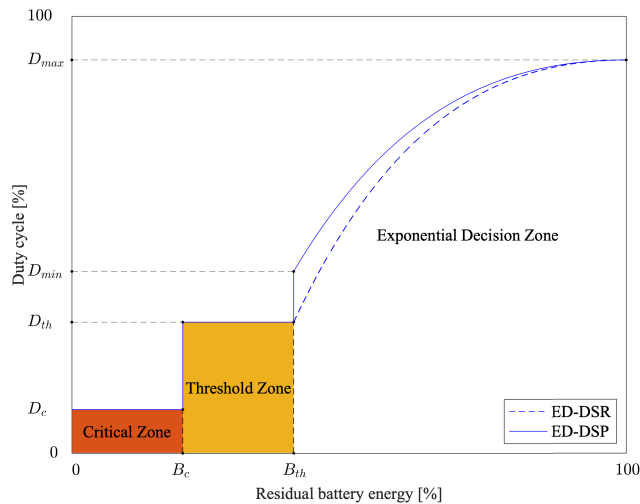
FIGURE 2. A decision graph of the ED-MAC protocol.

According to the S-MAC protocol, Fig. 1 depicts a scenario of node A sending a message to node B in one duty cycle. In active mode, the schedules of nodes A and B first have to be updated with SYNC packages. If nodes A and B are on the same schedule, node A will send an RTS (Request to send) package to node B. If node B is ready to receive data, it will respond with a CTS (Clear to send) package to node A. Then, node A will transmit data to node B. When node B finishes receiving the data, it will send an ACK (Acknowledge) package to indicate the end of the process. After that, both nodes will enter sleep mode.

MAC protocols for WSNs are continuously being improved in throughput, latency, and energy consumption, for example, T-MAC, B-MAC, WiseMAC, X-MAC, RI-MAC, PW-MAC, WX-MAC, SW-MAC, and DS-MAC protocol [9]. An energy harvesting technology can be applied to transmit more data using the same battery size. In 2014, exponential decision MAC (ED-MAC) protocols for SEH-WSNs were proposed [7]. Their mechanism is to adjust the duty cycle following the exponential slope depending on the battery energy as shown in Fig. 2. There are two types of ED-MAC protocols. One is the exponential decision-dynamic duty cycle scheduling based on current residual energy (ED-DSR), and the other is based on prospective increase in energy (ED-DSP).

To prevent battery depletion, the ED-MAC protocols are organized into 3 decision zones as shown in Fig. 2. It consists

of an axis x representing residual battery energy B_r and an axis y representing a duty cycle of the ED-MAC protocols corresponding to the residual battery energy. The first zone is a critical zone (red area). When the battery energy is below a critical battery level B_c, the duty cycle is set at a critical duty cycle level D_c. The critical duty cycle level is very low or can be zero to save battery energy. The second zone is a threshold zone (yellow area). When the battery energy is between the critical battery level and a threshold battery level B_{th}, the duty cycle is set at a threshold duty cycle level D_{th}. This duty cycle level is higher than the critical level but not too high in order to send data at a constant rate and save more energy. The final zone is an exponential decision zone. In this zone, the duty cycle is adjusted according to an exponential curve depending on the types of the ED-MAC protocols. One is the ED-DSR (dashed line in Fig. 2). The duty cycle changes when the residual battery is low, and also gradually changes when the residual battery is high. The other is the ED-DSP (solid line in Fig. 2). Since the node can harvest energy, the ED-DSP makes decisions with the residual battery plus expected harvested energy E_e. Therefore, the exponential curve of the ED-DSP is higher than the ED-DSR, which means that the node is allowed to have a higher duty cycle. As the result, the data transfer rate of the ED-DSP is higher than the ED-DSR.

The mathematic representation of ED-DSP can be expressed as: (1).

$$D_{ED-DSP} = D_{min} + \alpha\gamma e^{-\gamma} \qquad (1)$$

where D_{max} and D_{min} are the maximum and minimum duty cycle on the D_{ED-DSP} curve, $\alpha = (D_{max} - D_{min})e^1$, $\gamma = \frac{(B_r+E_e)-B_{th}}{(B_{max}+E_e)-B_{th}}$, and $B_r \in [B_{th}, B_{max}]$.

If the expected harvested energy is zero, the ED-DSP equation becomes the ED-DSR equation because it considers only the residual energy.

Hence, the most challenge for the ED-DSP is the precise prediction of the expected harvested energy due to the uncertainty of the weather conditions. Table 2 shows the prediction techniques used to forecast solar irradiance.

However, the prediction methods in Table 2 also have the prediction error. Therefore, this article presents the MDP policy which does not use the prediction in its mechanism. To compare performance between MDP policy and ED-DSP, we use the ideal prediction for the ED-DSP to forecast the expected harvested energy, so that the expected harvested energy at time t perfectly equals the charged energy at time $t+1$. The next subsection presents the examples of SEH-WSN nodes.

C. SEH-WSN NODES
In [17], R. Belu designed and analyzed a micro-solar power for WSNs. The SEH-WSN node is designed to harvest solar energy. The node consists of a mini-PV panel, primary buffer super-capacitors, and a secondary buffer rechargeable battery. Consequently, Two 22F/2.5V super-capacitors can supply the power for 10 hours with no sunlight. However, this article will
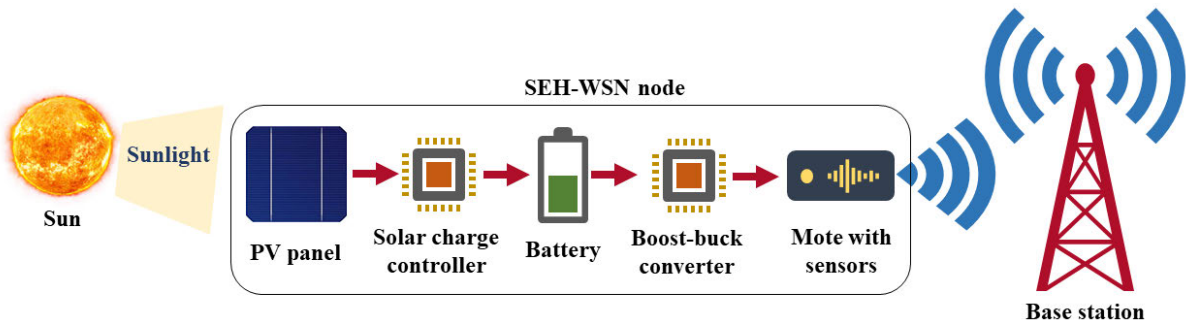
FIGURE 3. A structure of the SEH-WSN node [18].

TABLE 2. Prediction techniques for predicting solar irradiance.

Prediction technique	Year	Detail
Exponential weighted moving-average (EWMA)	2007	A. Kansal et al. utilized the EWMA filter to predict solar energy used for energy management in sensor networks [10].
Weather-conditioned moving average (WCMA)	2009	J. R. Piorno et al. presented the adaptation of the EWMA called WCMA which estimates the current energy from the averge of the last harvested energy and the average harvested energy in the past days with the dynamic weight [11].
Accurate solar energy allocation (ASEA)	2011	D. K. Noh and K. Kang proposed an advanced expectation model of harvested energy to manage the energy in each time slot [12].
PROfile energy (Pro-energy)	2012	A. Cammarano et al. proposed the Pro-energy to predict the solar and wind energy for WSNs. It has better performance than EWMA and WCMA [13].
Q-learning	2016	S. Kosunalp proposed a solar energy prediction via Q-learning. The Q-leaning method outperforms the EWMA, WCMA, ASEA, and Pro-energy in both time slots and months [14].
Real-forecast weather moving average (RWMA)	2018	H. Ren et al. presented the RWMA improved the accuracy when the weather rapidly changes. It yields an average daily error of only 11% while the EWMA and WCMA have an average daily error of 56% and 31% respectively [15].
Autoregressive moving-average (ARMA)	2020	I. SANSA et al. simulate the ARMA on a winter day. As the result, the prediction error does not exceed 10% [16].

TABLE 3. Advantages and disadvantages of different battery types [18], [19].

Battery types	Advantage	Disadvantage
Lithium-Ion (Li-ion)	Long life cycle Low self-discharge rate	Expensive Small capacity Complex charging circuit
Nickel Cadmium (NiCd)	Deliver fill rated capacity	Temporary capacity loss Fast discharge rate
Nickel Metal Hydride (NiMH)	High energy density	Low life cycle than Li-Ion
Thin film	High cell voltage Long life cycle	Small capacity High internal resistance
Ultra-capacitors	High power density Long life cycle	High self-discharge rate Small capacity

is used to step down the voltage from the 3.7V battery to the mote.

In [19], L. J. Chen *et al.* experimented on a simple SEH-WSN node, and also provided essential guidance for designing an SEH-WSN node. The designed node consists of a 114.3mmx66.8mm 3.3V PV panel from the BP Solar model MSX-005F, two AA 2.5V 750mAh NiMH batteries from Energizer model NM15, and a MICAz mote with a board model MDA300. a Schottky diode is used as a solar charge controller. Its function is not to step down the voltage, but to prevent the reverse current from the battery to the PV panel in the event of insufficient solar irradiance to charge the battery.

The advantages and disadvantages of different battery types are shown in Table 3. There is currently no battery type that has all the advantages in terms of cost, energy density, power density, life cycle, self-discharge rate, and others. For example, Li-ion, thin film, and ultra-capacitors have a long life cycle but have a small capacity. In contrast, NiMH has high energy density but has a low life cycle. This article requires a battery that has a long life cycle, small capacity, and very low self-discharge rate which can be ignored in a calculation. This requirement is close to the capabilities offered by the Li-ion battery.

D. SOLAR IRRADIANCE AND SOLAR CHARGING MODELS
In [20], a cloudy sky irradiance model was proposed. This model was developed from the simple clear sky model expressed in (2). The clear sky model utilizes the part of a sine function starting from the angle at 0 to π radians to present

address the uncertainty of solar irradiance, a challenge that does not possess an optimal solution, as of yet.

In [18], Hong *et al.* presented the design and implementation of an SEH-WSN node used for logging solar irradiance. The designed SEH-WSN node, as shown in Fig. 3, is composed of a PV panel, a solar charge controller, a battery, a boost-buck converter, and a mote with sensors. The design is based on a MICAz mote that needs 2.7 - 3.3 V supply voltage. The selected PV panel has a 10cmx10cm size with 13% efficiency. A LT3652 step-down battery charger from Liner Technology Corporation (LTC) is used as the solar charger controller in order to step down the voltage from the 9V PV panel to a 3.7V 2,500mAh Li-ion battery. Then, a LTC3440 high efficiency boost-buck converter from LTC

TABLE 4. An example of cloudy model parameters with the $k_D - POP_D$ solar irradiance classification.

Class	Description		Cloudy Model Parameter						
	Quantity	Quality	F	a_1	b_1	c_1	a_2	b_2	c_2
1	High	High	1	0.25	5	3	0	0	0
2	Medium	High	1	0.5	5	3	0	0	3
3	Low	High	0.25	0.5	5	3	0	0	3
4	High	Medium	1	0.5	5	50	0	0	3
5	Medium	Medium	0.9	1	5	3	0	0	3
6	Low	Medium	-	-	-	-	-	-	-
7	High	Low	-	-	-	-	-	-	-
8	Medium	Low	1	0.5	13	3	0	0	3
9	Low	Low	-	-	-	-	-	-	-
10	-	Very Low	1	0.5	50	3	0	0	3

the clear sky irradiance I_{clear} from sunrise time t_{rise} to sunset time t_{set} in an hour.

$$I_{clear}(t) = I_{max} \sin\left(\frac{\pi(t - t_{rise})}{t_{set} - t_{rise}}\right), \quad t_{rise} < t < t_{set} \quad (2)$$

In (2), the maximum solar irradiance I_{max} is the multiplication of a cloudy sky factor F and a daily maximum extraterrestrial irradiance $I_{ETI_{max}}$ expressed in (3). The maximum extraterrestrial irradiance depends on a solar zenith angle and is simply set as 1,362W/m^2. The cloudy sky factor has range from 0 to 1. Hence, a higher value means a clearer sky.

$$I_{max} = FI_{ETI_{max}} \quad (3)$$

The cloudy model is adapted from the simple clear sky model by modifying the smooth half-circle by adding the extra sinusoidal terms expressed in (4). Consequently, the added terms affect three components: 1) the amplitude depending on the parameters a, 2) the number of ripples on the curve depending on the b, and 3) the size of the ripples depending on the parameters c. The absolute operations are used to prevent the negative amplitude.

$$I_{cloudy}(t) = I_{clear}\left(1 - a_1 \left|\sin\left(b_1\frac{\pi(t - t_{rise})}{t_{set} - t_{rise}}\right)\right|^{c_1} \right.$$
$$\left. - a_2 \left|\sin\left(b_2\frac{\pi(t - t_{rise})}{t_{set} - t_{rise}}\right)\right|^{c_2}\right), \quad t_{rise} < t < t_{set} \quad (4)$$

This model can generate the solar irradiance in classes 1-5, 8, and 10 following $k_D - POP_D$ the classification proposed in [21] by varying the parameters F, a, b, and c as shown in Table 4. The $k_D - POP_D$ is created base on a daily clearness index k_D and daily probability of persistence POP_D to indicate the quantity and quality of solar irradiance. On the one hand, high quantity means a high amount of solar irradiance obtained on the ground. On the other hand, high quality means low fluctuation of solar irradiance.

Fig. 4 shows hourly solar irradiance graph in classes 1-5, 8, and 10. These solar irradiance are computed with maximum extraterrestrial irradiance equal to 1,362W/m^2, sunrise time at 6 AM, sunset time at 6 PM, and other parameters in Table 4.

A simple model of converting solar irradiance to battery energy is depicted in Fig. 5. There are two processes in
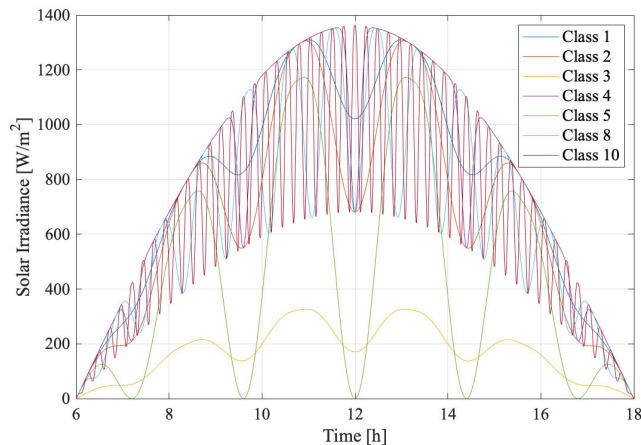
FIGURE 4. Hourly solar irradiance in classes 1, 2, 3, 4, 5, 8, and 10 with the maximum extraterrestrial irradiance at 1,632W/m^2.
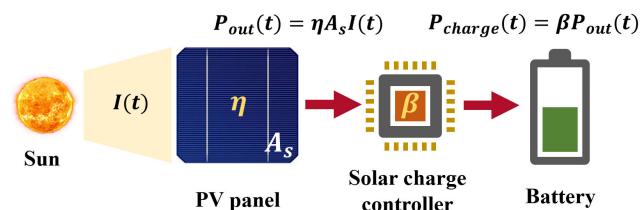
FIGURE 5. A simple model of converting solar irradiance to battery energy.

this model. First, solar energy is converted to electrical energy by the PV panel. Second, the electrical energy is charged into the battery by a solar charge controller.

When sunlight reaches the PV panel with size A_s and efficiency η, the solar irradiance I is converted to electrical power P_{out}. This process can be expressed in (5). In [22], there is a wide range of efficiency from 7.1% to 47.1% depending on PV types.

$$P_{out}(t) = \eta A_s I(t) \quad (5)$$

After the electrical power P_{out} is produced by the PV panel, it will pass through the solar charge controller with efficiency β to charge the battery. Hence, the potential power charged into the battery can be expressed as (6). In [23], the efficiency of the charging circuit normally is 80% and can increase to 89% by using a supercapacitor instead of a conventional capacitor.

$$P_{charge}(t) = \beta P_{out}(t) \quad (6)$$

Therefore, the potential power charged into the battery at time t can be expressed as (7).

$$P_{charge}(t) = \beta\eta A_s I(t) \quad (7)$$

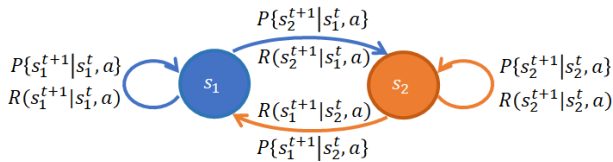In addition, the potentially charged energy in the entire day can be expressed as (8).

$$E_{charge_{day}} = 3,600\beta\eta A_s \int_{t_{rise}}^{t_{set}} I(t)dt \quad (8)$$

TABLE 5. Potentially charged energy in the entire day and the different irradiance classes.

Class	Energy [J]
1	14,501
2	12,757
3	3,189
4	15,318
5	8,343
8	12,792
10	12,797
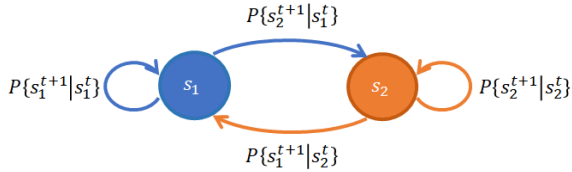
FIGURE 6. Two-state Markov chain.

FIGURE 7. Two-state Markov chain with action parameter in reward function.

FIGURE 8. A system model.

FIGURE 9. An SEH-WSN structure.

Table 5 presents the amount of the potentially charged energy in the entire day calculated by the same parameters in Fig. 4. Class 1 and 2 (high quantity) irradiance models have higher energy than others, but the irradiance class 1 (high quality) has a smoother curve than the class 4 (medium quality). The irradiance class 3 (low quantity) has the minimum energy. The irradiance class 10 (very low quality) has many ripples on the irradiance curve.
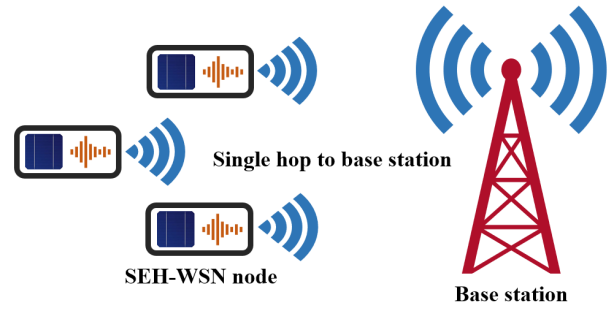
E. MARKOV DECISION PROCESS

MDP is a discrete-time stochastic process and is applied from a Markov chain. It can be used to solve the optimization problem. The Markov chain is a diagram consisting of states s, arrow lines (from one state at the current timestep t to another state at the next timestep $t + 1$), and probability P corresponding to the arrow line as shown in Fig. 6.
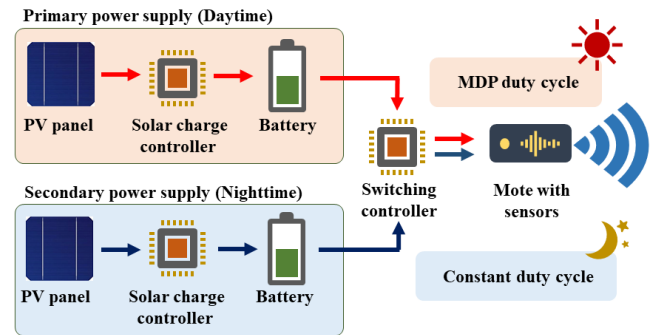
The two-state Markov chain, in Fig. 6, consists of states s_1 and s_2. The states s_1 and s_2 at time t can remain in the same state or move to another state at time $t + 1$. The transitions of the states can be indicated by the arrow lines corresponding to the transition probability $P\{s^{t+1}|s^t\}$. Therefore, the summation of $P\{s_1^{t+1}|s_1^t\}$ and $P\{s_2^{t+1}|s_1^t\}$ and the summation of $P\{s_2^{t+1}|s_2^t\}$ and $P\{s_1^{t+1}|s_2^t\}$ are equal to one. The transitions of these states are considered only two timesteps: one is the current time step and two is the next timestep.

To link the Markov chain and the MDP, an action parameter a and a reward function $R(s^{t+1}|s^t, a)$ are added in the diagram as shown in Fig. 7.

Although the MDP was discovered many decades ago, its applications remain useful in many fields of study such as optimal service auction for sensor-as-a-service [24], network selection in 5G [25], optimization of uplink outage probability and throughput of cellular IoT networks [26], and optimization of video streaming [27]. This article applies the MDP to optimize data transfer and prevent battery depletion for an SEH-WSN node. The proposed system model and method are described in the next section.

III. SYSTEM MODEL

The SEH-WSN model used in this article, as shown in Fig. 8, consists of a base station and SEH-WSN nodes. The SEH-WSN nodes directly communicate to the base station in a single hop fashion.

The SEH-WSN node consists of a primary power supply, a secondary power supply, a lossless switching control, and a mote with sensors, as shown in Fig. 9. The power supply is separated into 2 sections for use in the daytime and nighttime because the MDP policy is applied only in the daytime. In the nighttime, a constant duty cycle was set since no solar energy harvesting takes place. Thus, the secondary battery has a fixed consumption rate. To switch the power sources between the primary and secondary, the switching controller is used. It will switch to the second power source by sensing the charging rate into the battery. If it notices that there is no charging, the mote will be supplied by the secondary power source.

In the daytime, the SEH-WSN node is programmed with an MDP policy to decide an action according to the current state of the SEH-WSN node as shown in Fig. 10. The process initially checks the state of the SEH-WSN node referring to a battery level and a duty cycle level. Subsequently, the node
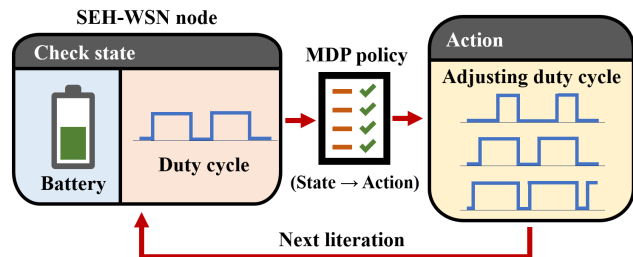
FIGURE 10. A process of adjusting a duty cycle.

will map the current state to the action in the MDP policy programmed in the node's memory. Then, the node will adjust the duty cycle according to the policy. There are 3 actions designed into this model: 1) decreasing the duty cycle, 2) maintaining the current duty cycle, and 3) increasing the duty cycle. After that, the node will repeat the process.

Using the MDP policy contained in the node's memory can save computing energy in a processor because it only operates the mapping process to make the optimal decision. The next section proposes a method to compute an MDP policy.

IV. PROPOSED METHOD
The MDP policy, meaning and mathematical model of a state set, an action set, transition probability matrices, and reward vectors can be computed as follows:

A. STATE SET
State set is a set of all the possible statuses of the SEH-WSN node. The status is a pair of a battery energy level and a duty cycle level. The state set can be written as (9)

$$\mathscr{S} = \{\mathscr{B}, \mathscr{D}\} \tag{9}$$

where $\mathscr{B}$ is a set of battery energy level that has M levels. Then, the set of battery energy level can be expressed as $\mathscr{B} = \{b_1 = 0J, b_2, b_3, \ldots, b_m, \ldots, b_M = B_{max}\}$. $\mathscr{D}$ is a set of duty cycle level that has N levels. Then, the set of duty cycle level can be expressed as $\mathscr{D} = \{d_1 = 0\%, d_2, d_3, \ldots, d_n, \ldots, d_N = 100\%\}$.

In (9), the number of all possible states equals to M x $N = Z$. Moreover, the state set can be expressed in (10).

$$\mathscr{S} = \{s_1, s_2, s_3, \ldots, s_z, \ldots, s_Z\} \tag{10}$$

where s_z is an zth state that has a pair of the battery and duty cycle level (b_m, d_n).

The relation between battery energy level M and duty cycle level N is simply set by Condition 1 that one level of duty cycle consumes one level of the battery energy.

Condition 1: Battery energy in one level is equal to energy consumption due to one level of duty cycle.

The energy consumption occurs due to mote calculation and transmission in each duty cycle D. The consumed energy can be written as a function of a duty cycle by considering the power consumption in active mode P_{active} and sleep mode P_{sleep}. Then, we can express the maximum energy

consumption in one operation period T_{opt} in (11).

$$E_{cons}(D) = \frac{[DP_{active} - (100 - D)P_{sleep}]T_{opt}}{100} \tag{11}$$

Thus, the maximum energy consumption occurs at the duty cycle equal to 100% and can be expressed as (12).

$$E_{cons_{max}} = P_{active}T_{opt} \tag{12}$$

B. ACTION SET
The amount of data transfer depends on a duty cycle. When the duty cycle increases, there is more chance for transmitting data. In addition, the high duty cycle can cause battery depletion. Hence, in this model, an action set $\mathscr{A}$ is designed to control the duty cycle to maximize the chance of data transfer and also prevent the depletion of the battery. The action set consists of an action parameter a to control the duty cycle and is expressed as (13).

$$\mathscr{A} = \{a \,|\, a \text{ is an integer parameter}\} \tag{13}$$

The parameter a is the action variable that presents the change of duty cycle in 3 actions as shown in (14).

$$a = \begin{cases} -1, & \text{decreasing the duty cycle} \\ 0, & \text{remaining the duty cycle} \\ 1, & \text{increasing the duty cycle} \end{cases} \tag{14}$$

C. TRANSITION PROBABILITY MATRICES
The transition probability matrix denoted by $\boldsymbol{T}_P(a)$ is the probability that indicates a change from the ith current state s_i to the jth next state s'_j by taking an action a. Therefore, the transition probability matrix can be expressed as a square matrix that shows the probability of change from the current states assigned as the ith row mapping to the next states assigned as the jth column shown in (15).

$$\boldsymbol{T}_P(a)$$
$$= \begin{bmatrix} P\{s'_1|s_1, a\} & P\{s'_2|s_1, a\} & \cdots & P\{s'_J|s_1, a\} \\ P\{s'_1|s_2, a\} & P\{s'_2|s_2, a\} & \cdots & P\{s'_J|s_2, a\} \\ \vdots & \vdots & \ddots & \vdots \\ P\{s'_1|s_I, a\} & P\{s'_2|s_I, a\} & \cdots & P\{s'_J|s_I, a\} \end{bmatrix}_{I \times J} \tag{15}$$

In this model, the change of state depends on two factors. One is the change of the duty cycle in each action, and the other is the probability of solar irradiance. Therefore, to model the transition probability matrices, building duty cycle transition probability matrices with the action a is initiated. Next is building battery energy transition probability matrices. Finally, the completed transition probability matrices are constructed by combining the duty cycle transition probability matrices with the battery energy transition probability matrices.

1) DUTY CYCLE TRANSITION PROBABILITY MATRICES
The duty cycle transition probability matrices denoted by $\boldsymbol{T}_D(a)$ present the probability of change from the current duty cycle at nth row (d_n) to the next duty cycle at uth column

(d'_u) when the node implements the decision a. Hence, it can be classified into 3 cases: a equals to -1, 0 and 1. When the node decides to decrease or increase the duty cycle, the duty cycle is only changed in one duty cycle level. Hence, the duty cycle transition probability matrices becomes or similar to the identity matrix shown in (16).

$$
\mathbf{T}_D(a) = \begin{cases} 1 & \text{when } u = n + a, \forall a \\ 1 & \text{when } u = n = 1, a = -1 \\ 1 & \text{when } u = n = N, a = 1 \\ 0 & \text{otherwise} \end{cases} \tag{16}
$$

Case 1: Decrease duty cycle ($a = -1$)

In this case, the duty cycle is decreased by one level, so that the probability mapping from d_n to d'_u equals to one only in the case $u = n - 1$ and the other cases are zero. The $\mathbf{T}_D$ can be expressed in (17).

$$
\mathbf{T}_D(-1) = \begin{bmatrix} 1 & & & \\ 1 & & & \\ & 1 & & \\ & & \ddots & \\ & & & 1 \end{bmatrix}_{N \times U} \tag{17}
$$

Case 2: Stay in the same duty cycle ($a = 0$)

In this case, the duty cycle remains in the same duty cycle, so that the probability mapping from d_n to d'_u equals to one only in the case $u = n$ and the other cases are zero. The $\mathbf{T}_D$ becomes the identity matrix shown in (18).

$$
\mathbf{T}_D(0) = \begin{bmatrix} 1 & & & & \\ & 1 & & & \\ & & 1 & & \\ & & & \ddots & \\ & & & & 1 \end{bmatrix}_{N \times U} \tag{18}
$$

Case 3: Increase duty cycle ($a = 1$)

In this case, the duty cycle is increased by one level, so that the probability mapping from d_n to d'_u equals to one only in the case $u = n + 1$ and the other cases are zero. The $\mathbf{T}_D$ can be expressed in (19).

$$
\mathbf{T}_D(1) = \begin{bmatrix} & 1 & & & \\ & & \ddots & & \\ & & & 1 & \\ & & & & 1 \\ & & & & 1 \end{bmatrix}_{N \times U} \tag{19}
$$

2) BATTERY ENERGY TRANSITION PROBABILITY MATRIX

The battery energy transition probability matrix is denoted by $\mathbf{T}_B$. This matrix expresses the probability of changing from the mth current battery energy b_m to the vth next battery energy b'_v corresponding to solar irradiance and energy consumption. The solar irradiance yields the battery energy remaining or increasing. In contrast, the duty cycle causes the reduction of battery energy due to data transmission and computation.

Solar irradiance can potentially charge the battery with a varying amount of energy depending on the weather

TABLE 6. Algorithm for calculation of the potentially charged energy probability.

Algorithm 1 Calculation of potentially charged energy probability
1 : Initialize solar irradiance parameters : $I_{max}, t_{rise}, t_{set}, F, a_1, b_1, c_1, a_2, b_2, c_2,$
2 : Initialize PV panel and charging control parameters : η, A_s, β
3 : Initialize potentially charged energy probability level : W
4 : Calculate potentially charged energy probability in each level : $E_{charge}(w) = (w - 1)\frac{E_{charge\,max}}{W-1}$
5 : Set time index $t = [t_{rise}:$increment$:t_{set}]$
6 : Calculate potentially charged energy at time t : $E_{charge}(t) = \beta\eta A_s T_{opt} I_{cloudy}(t)$
7 : Set count vector : $count = \text{zeros}(1, W)$
8 : for $k = 1$: size(time index)
9 :   for $w = 1 : W$
10 :   if $E_{charge}(k) \leq E_{charge}(w)$
11 : $count(w) = count(w) + 1$
12 :   break
13 :   end if
14 :   end for
15 : end for
16 : $P_p(w) = \frac{count(w)}{\text{size(time index)}}$

conditions. Due to this uncertainty, a desecrate potentially charged energy probability density is applied in the battery energy transition probability matrix. This probability density can be written as a vector $\mathbf{P}_p$ and expressed in (20).

$$
\mathbf{P}_p = \begin{bmatrix} P_{p_1}, P_{p_2}, \ldots, P_{p_w}, \ldots, P_{pW} \end{bmatrix} \tag{20}
$$

where P_{p_w} is the potentially charged energy probability at level w of overall W levels. According to the property of the probability density, a summation of all members in $\mathbf{P}_p$ is equal to one. The potentially charged energy probability can be computed by quantizing the potentially charged energy function from (8) into W levels. Then, counting the number of the charge energy occurring in each level. Finally, the potentially charged energy probability is equal to the faction of the number of occurrences over the total time samples as shown in Table 6.

In this model, the relation between the number of the potentially charged energy probability W and the number of the duty cycle level N is set by Condition 2.

Condition 2: Charged energy in one level equals to the energy consumption in one level.

This condition shows that the battery energy will increase due to the charged energy from the potentially charged energy probability, but will decrease due to the energy consumption from the duty cycle. Thus, the battery energy transition probability matrix can be expressed in (21).

$$
\mathbf{T}_B(b'_v|b_m, d'_u)
$$
$$
= \begin{cases} P_{p_w} & \text{when } v = m + \text{w-}u \\ & \cap v \neq 1 \cap v \neq V \\ 1 - \sum T_B(m, 2 : V) & \text{when } v = 1 \\ 1 - \sum T_B(m, 1 : V - 1) & \text{when } v = V \\ 0 & \text{otherwise} \end{cases} \tag{21}
$$

where $\sum T_B(m, 2 : V)$ is the summation of elements in the mth row from 2nd column to Vth column, and

	b'_1	b'_2	b'_3	b'_4	b'_5	b'_6	b'_7
b_1	$1 - P_{p_3}$	P_{p_3}					
b_2	$1 - (P_{p_2} + P_{p_3})$	P_{p_2}	P_{p_3}				
b_3		P_{p_1}	P_{p_2}	P_{p_3}			
b_4			P_{p_1}	P_{p_2}	P_{p_3}		
b_5				P_{p_1}	P_{p_2}	P_{p_3}	
b_6					P_{p_1}	P_{p_2}	$1 - (P_{p_1} + P_{p_2})$
b_7						P_{p_1}	$1 - P_{p_1}$

FIGURE 11. An example of the battery energy transition probability matrix.

$\sum T_B(m, 1 : V - 1)$ is the summation of elements in the mth row from 1st column to $(V - 1)$th column. In Fig. 11, the example of the battery energy transition probability matrix with $M = 7$, $W = 3$, and $u = 2$ is presented.

3) TRANSITION PROBABILITY MATRICES
The complete transition probability matrices are the combination of the duty cycle transition probability matrices and the battery energy transition probability matrices by using Kronecker product shown in (22).

$$\mathbf{T}_P(s'_j|s_i, a) = \mathbf{T}_D(d'_u|d_n, a) \otimes \mathbf{T}_B(b'_v|b_m, d'_u)$$

$$= \begin{cases} T_B(b'_v|b_m, d'_u) & \text{when } u = n + a, \forall a \\ T_B(b'_v|b_m, d'_u) & \text{when } u = n = 1, a = -1 \\ T_B(b'_v|b_m, d'_u) & \text{when } u = n = M, a = 1 \\ 0 & \text{otherwise} \end{cases}$$

$$(22)$$

One property of the transition probability matrix is the summation of each row equal to one due to the summation of each row in (16) and in (21) equal to one.

D. REWARD VECTORS
A reward is an amount of data transfer depending on the state s and action a and denoted by a vector $\mathbf{R}(s, a)$. The number of elements equals to L and the order of reward elements corresponding to the order of the state set $\mathcal{S}$. Hence, L equals to $M \times N$ and the reward vectors can be written as (23).

$$\mathbf{R}(s, a)$$
$$= [r(1, a), r(2, a)_2, r(3, a)_3, \ldots, r(l, a), \ldots, r(L, a)]$$

$$(23)$$

where $r(l, a)$ is a lth state of reward vectors belonging to action a. In addition, l also represents the pair of the battery energy level and the duty cycle level (b, d), and can be

expressed as (24).

$$1, 2, 3, \ldots, l, \ldots L$$
$$= (b_1, d_1), (b_2, d_1), \ldots, (b_m, d_1), \ldots, (b_M, d_1),$$
$$(b_1, d_2), (b_2, d_2), \ldots, (b_m, d_n), \ldots, (b_M, d_N) \quad (24)$$

The data will be transmitted to the base station if the duty cycle is greater than 0% and there is sufficient supply energy. The supply energy is from the battery energy B and the charged energy E_{charge}. Hence, there are 2 cases that reward will occur. In the first case, the supply energy is greater than the consumed energy. In the second case, the supply energy is less than the consumed energy, but not equal to zero. Therefore, the reward can be expressed as (25).

$$R(s, a) = \begin{cases} DD_{tr}T_{tr} & \text{when } n + a > 1 \cap \\ & (m > 1 \cup w > 1) \quad (25) \\ 0 & \text{otherwise} \end{cases}$$

where D is the duty cycle, D_{tr} is the data transfer rate, and T_{tr} is the time for transmitting data as expressed in (26).

$$T_{tr} = \frac{B + P_p P_{charge} T_{act}}{P_{cons}} \quad (26)$$

where P_{charge} is the charged power from the PV panel. T_{act} is the active time period. P_{cons} is the power consumption generally from computation and communication. Then, (25) and (26) yield the reward equation in (27).

$$R = DD_{tr} \frac{B + P_p P_{charge} T_{act}}{P_{cons}} \quad (27)$$

E. OPTIMIZATION FORMULATION AND SOLUTION
The goal of solving the MDP is to obtain a policy that yields the optimum solution. In [28], linear programming technique is presented as a solution to solve the MDP problem. This method is applied for Discrete Time Markov Decision Process in an infinite horizon problem. To compute the MDP policy, the optimization problem shown in (28) is to maximize the reward in every state and action. This solution will yield the optimal solution of the randomized policy or decision variable $\phi(s_i, a)$ defined as the probability of the ith state with action a occurs.

$$\max_{\phi(s_i, a)} \sum_{s_i \in \mathcal{S}} \sum_{a \in \mathcal{A}} \phi(s_i, a) R(s_i, a),$$

$$\text{s.t. } \sum_{a \in A} \phi(s'_j, a) = \sum_{s_i \in \mathcal{S}} \sum_{a \in \mathcal{A}} \phi(s_i, a) \mathbf{T}_P(s'_j|s_i, a), \ s'_j \in \mathcal{S},$$

$$\sum_{s_i \in \mathcal{S}} \sum_{a \in \mathcal{A}} \phi(s_i, a) = 1, \phi(s_i, a) \geqslant 0 \quad (28)$$

This problem can be solved by linear programming and the result is the optimal randomized policy $\phi^*(s_i, a)$. Then, to obtain an optimal policy $\pi^*(s_i, a)$, each optimal randomized policy has to be normalized by the summation of the optimal randomized policy in the state for all actions as shown in (29).

$$\pi^*(s_i, a) = \frac{\phi^*(s_i, a)}{\sum_{a \in \mathcal{A}} \phi^*(s_i, a)} \quad (29)$$

TABLE 7. Algorithm for calculation of the MDP policy.

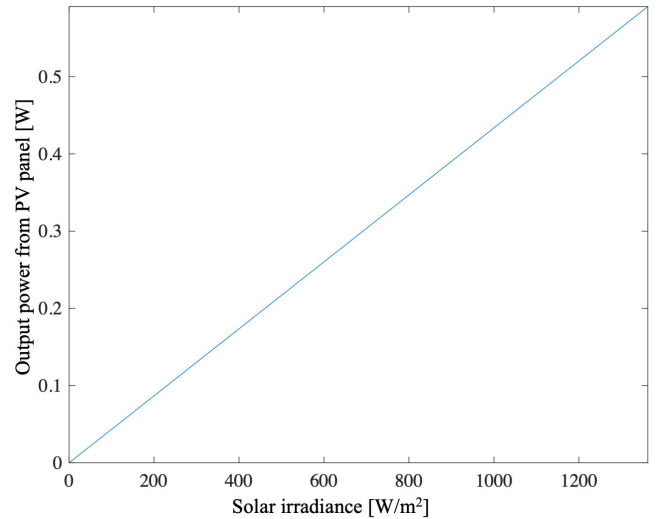| Algorithm 2 Calculation of the MDP policy |
|---|
| 1 : Initialise parameters: $M, N, W, B_{max}, a, D_{tr}$ |
| 2 : Calculate the potentially charged energy probability by Algorithm 1 |
| 3 : Calculate the transition probability matrices $\mathbf{T}_P$ by (22) |
| 4 : Calculate reward vector : $\mathbf{R}$ by (25) |
| 5 : Calculate the optimal randomized policy ϕ^* via linear programming by (28) |
| 6 : Calculate the optimal policy π^* by (29) |

Hence, the MDP policy can be computed by an algorithm shown in Table 7. First, essential parameters are required, such as the number of a duty cycle level, maximum energy consumption etc. Next, the numbers of battery energy level and potentially charged energy probability are computed by (18) and (28) respectively. Then, the number of potentially charged energy probability is used to compute potentially charged energy probability by Algorithm 1. After that, transition probability matrices and reward vectors are computed by (31) and (33) respectively. The optimization equation is formed by the transition probability and reward, and solved by linear programing to yield optimal decision variables in each state and action. Finally, they are normalized to obtain an optimal randomized policy or MDP policy.

V. POLICY EVALUATION

To assess the proposed model, first, the MDP policy has to be generated by Algorithm 2 as shown in Table 7. To form the proper MDP model, the outcome policy should be valid for almost all states. Thus, the number of battery energy levels has to be larger than the number of the duty cycle and potentially charged energy probability levels. Initially, the numbers of battery energy, duty cycle, and potentially charged energy levels are set to 27, 5, and 5 levels, respectively. The potentially charged energy probability is calculated from the clear sky model with maximum solar irradiance equal to the maximum extraterrestrial irradiance 1,362W/m^2, a cloudy factor equal to 1, sunrise time at 6 AM, and sunset time at 6 PM. The efficiency of the PV panel is set to the lowest efficiency 7.1% which is mentioned in the SEH-WSN nodes section. The panel size is 114.3mmx66.8mm following the MSX-005F model. A charge controller is set to 80% efficiency. Fig. 12 shows the conversion of solar irradiance into potentially charged power calculated by (7). The maximum solar irradiance at 1,362W/m^2 can potentially charge the battery at 0.59W.

The potentially charged energy probability is computed by Algorithm 1. Next, the data transfer rate is set to 250kbits/s which is from the transceiver of the MICAz mote to compute a reward. Finally, an MDP policy is generated by Algorithm 2.

After that, the MDP policy is simulated in different solar conditions and compared to the ED-DSP that has the ideal prediction. Hence, the expected harvested energy E_e of the

FIGURE 12. Conversion graph between solar irradiance and potentially charged power.

TABLE 8. Algorithm for simulation of the MDP policy and ED-DSP.

Algorithm 3 Simulation of the MDP policy and ED-DSP
1 : Initialise parameters: $I(t), B_{max}, B_{th}, B_c, D_{th}, D_c, A_s,$
: $\eta, \beta, D_{tr}, T_{opt}$
2 : for $t = t_{rise}$:increment:t_{set}
3 : Consider the duty cycle following the battery zone
: if $B(t) < B_c$
: $D(t) = D_c$
: else if $B(t) < B_{th}$
: if $D(t) < D_{th}$
: end if
4 : Calculate the energy consumption E_{cons} by (11)
5 : Calculate the potentially charged energy E_{charge} by (7)
6 : Calculate the battery energy for time $t + 1$
: $B(t + 1) = B(t) - E_{cons} + E_{charge}$
: and $0 \leq B(t + 1) \leq B_{max}$
7 : Make the decision via the MDP policy or ED-DSP
: to obtain $D(t + 1)$ and $0\% \leq D(t + 1) \leq 100\%$
8 : Calculate the amount of data transfer
9 : end for

ED-DSP is equal to the harvested energy in the next iteration. Algorithm 3 is used for the simulation, as shown in Table 8.

The parameters of the solar irradiance, PV panel, solar charge controller, mote, and transceiver used for simulation are shown in Table 9.

Then, we simulate the MDP policy and ED-DSP with the solar irradiance model parameters as shown in Table 4. They are simulated in different battery capacities and periods of daytime. First set of simulations, the period of daytime is constantly equal to 12h (6 AM-6 PM), and the battery capacity is changed from 50J to 150 and 500J. Second set of simulations, the battery capacity is constantly equal to 150J, and the period of daytime is changed from 10h (7 AM-5 PM) to 12h (6 AM-6 PM) and 14h (5 AM-7 PM). This simulations are focused on the amounts of data transfer and the behavior of battery energy and duty cycle during operation.

Next, we simulate the MDP policy and ED-DSP with real solar irradiance data for the entire year from the National Renewable Energy Laboratory (NREL) of the U.S.

TABLE 9. Initial parameters for evaluating the MDP model.

Parameter	Detail
Solar irradiance	
Classes 1-5, 8, and 10	Fig. 4
PV panel	
Dimensions	114.3mmx66.8mm
Efficiency	7.1%
Solar charge controller	
Efficiency	80%
Current draw in sleep mode	$<15\mu A$
Mote	
Current draw in an active mode	8mA
Current draw in a sleep mode	$<15\mu A$
Voltage for power supply	$<15\mu A$
Threshold and critical battery energy	30J and 10J
Threshold and critical duty cycle	10% and 0%
Transceiver	
Data transfer rate	250kbits/s
Current draw in active mode	19.7mA
Current draw in idle mode	$20\mu A$
Voltage for power supply	2.7-3.3V

Department of Energy in 4 different areas: 1) Golden, Colorado in 2019, 2) Eugene, Oregon in 2020, 3) Milford, Utah in 2012, and 4) Edinburg, Texas in 2017. The battery capacity used in these simulations is 50J. The results of the simulations are shown and discussed in the next section.

VI. RESULTS AND DISCUSSION

The results are presented in 3 parts. Part one is the results of generating the MDP policy. Part two is the results of simulating the MDP policy with the mathematical model comparing to the ED-DSP. The last part is the results of simulating the MDP policy with the real solar irradiance data comparing to the ED-DSP.

A. GENERATING OF MDP POLICY

The potentially charged energy probability used to generate the MDP policy calculated by Algorithm 1 is [0.1291 0.1332 0.1471 0.1818 0.4088]. Then, the parameters stated in section V are used to generate the MDP policy by Algorithm 2. Consequently, Fig. 13 depicts the policy of all states. The y axis represents actions -1, 0, and 1. The x axis represents states consisting of a battery energy level placed on the bottom and a duty cycle placed on the top. A circle represents the decision corresponding to the action and the state. Moreover, some states do not have a circle due to NaN value. The NaN occurs when the MATLAB is unable to define the numeric result, for example, 0 divided by 0. In this case, some states have the optimal randomized policy equal to 0 for all actions, and then the summation of the optimal randomized policy for all actions also equals 0. As a result, the normalized optimal randomized policy of this state equals NaN due to 0 divided by 0.

The policy can be completed by filling circles on the state that has the NaN value. The circle will be placed at the action -1 if the state is at a low battery energy level in order to save battery energy. In contrast, the circle will be placed at action
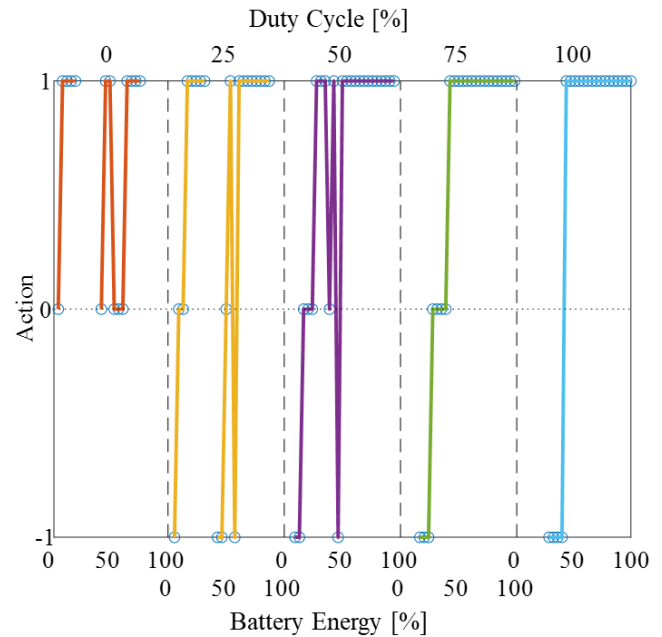
FIGURE 13. The optimal policy with $B_{max} = 150J$, $M = 27$, $N = 5$, and $W = 5$.
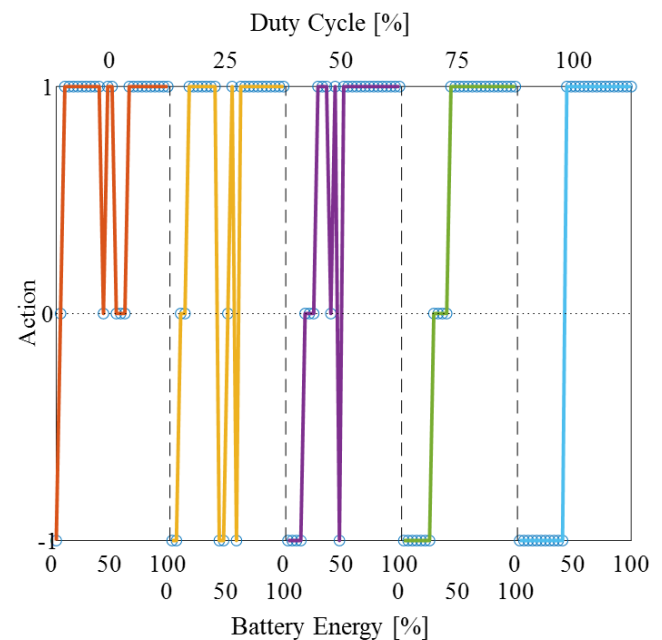
FIGURE 14. The complete optimal policy.

1 if the state is at a high battery level in order to increase data transmission. If the NaN occurs in the state that has the battery energy level in the middle range, the circle will be placed following the previous state decision. Therefore, the policy in Fig. 13 can be completed by filling the circle as shown in Fig. 14.

Next, the complete policy will be simulated to test the performance in different solar irradiance classifications, battery capacities, and periods of daytime. Furthermore, the MDP policy is compared to the performance of the ED-DSP.
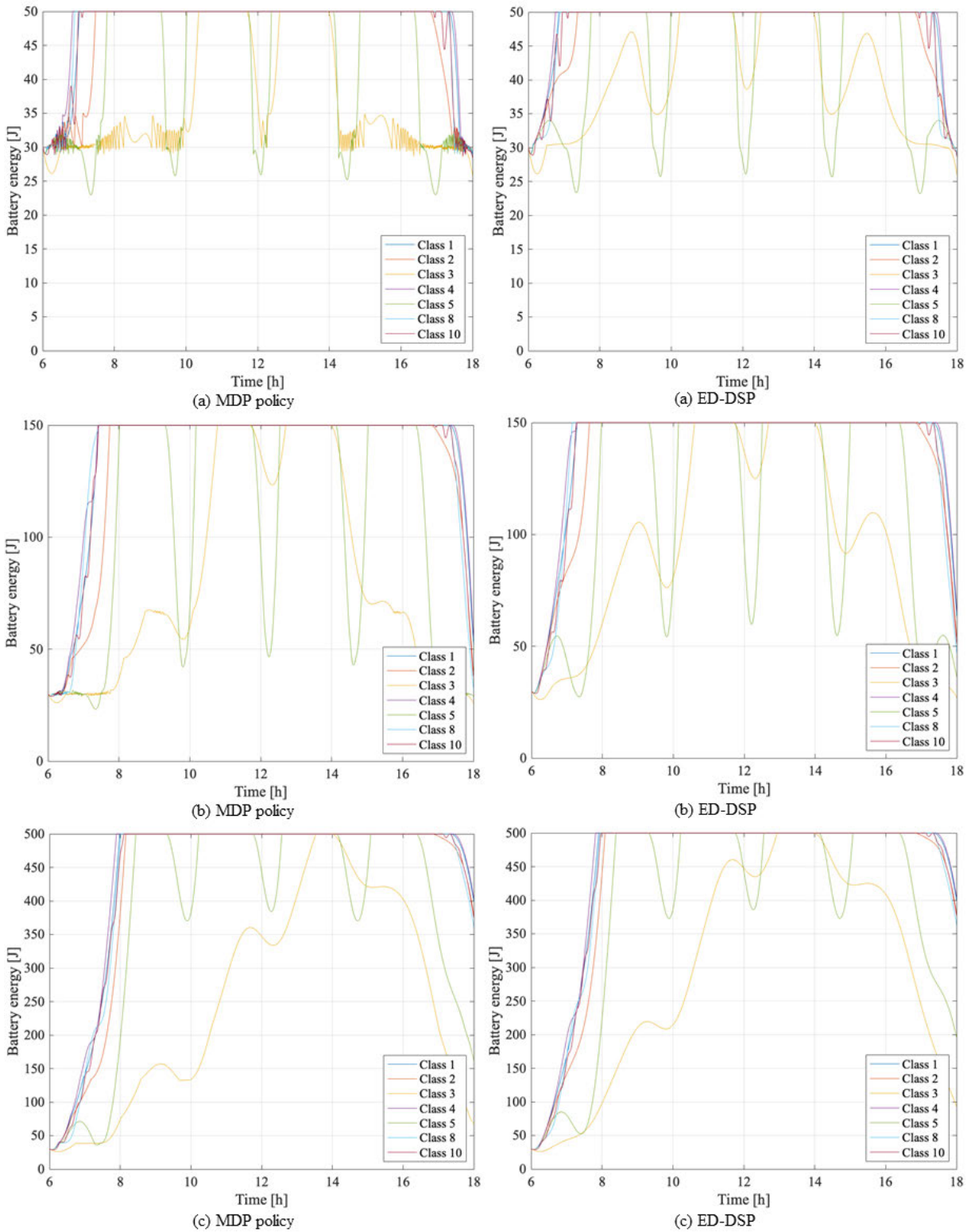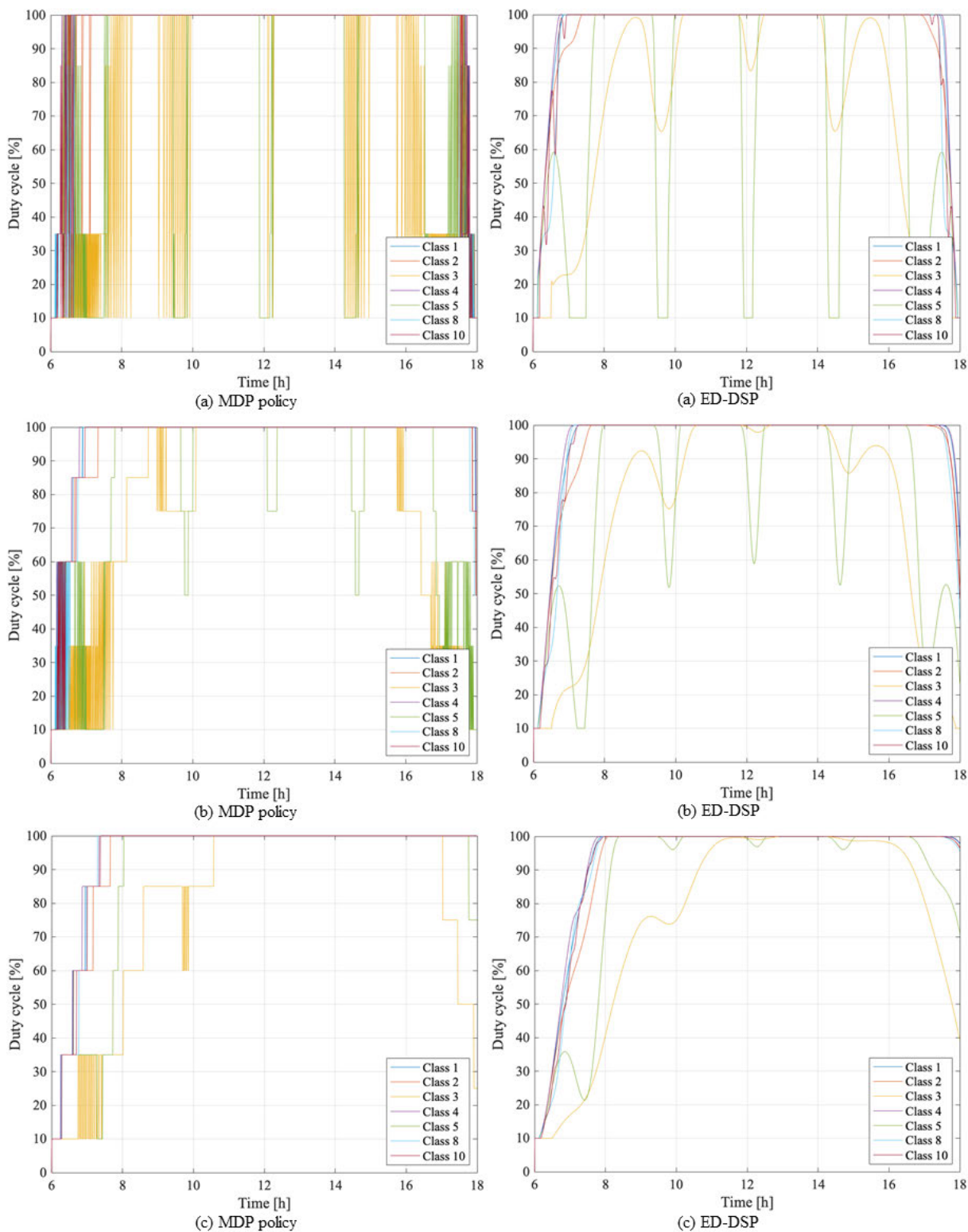
FIGURE 15. Graphs of the battery energy vs time of the MDP policy (left) and ED-DSP (right): (a) 50J, (b) 150J, and (c) 500J.

B. SIMULATION RESULTS WITH MATHEMATICAL MODEL
The simulation results of the node that has a battery capacity of 150J and operates from 6 AM to 6 PM are shown in Fig. 15 and Fig. 16.

Fig. 15 illustrates the residual battery energy during operations from 6 AM to 6 PM in the different battery capacities. No zero battery energy appears in both the MDP policy and ED-DSP. Therefore, both MDP policy and

FIGURE 16. Graphs of the duty cycle vs time of the MDP policy (left) and ED-DSP (right): (a) 50J, (b) 150J, and (c) 500J.

ED-DSP can be applied for practical use. The battery energy of the ED-DSP is smoother than the MDP policy because the ED-DSP gradually adjusts the duty cycle following

the residual energy following the exponential function. According to Table 5, the amounts of the potentially charged energy of the solar irradiance classes 1, 2, 4, 8, and 10 are
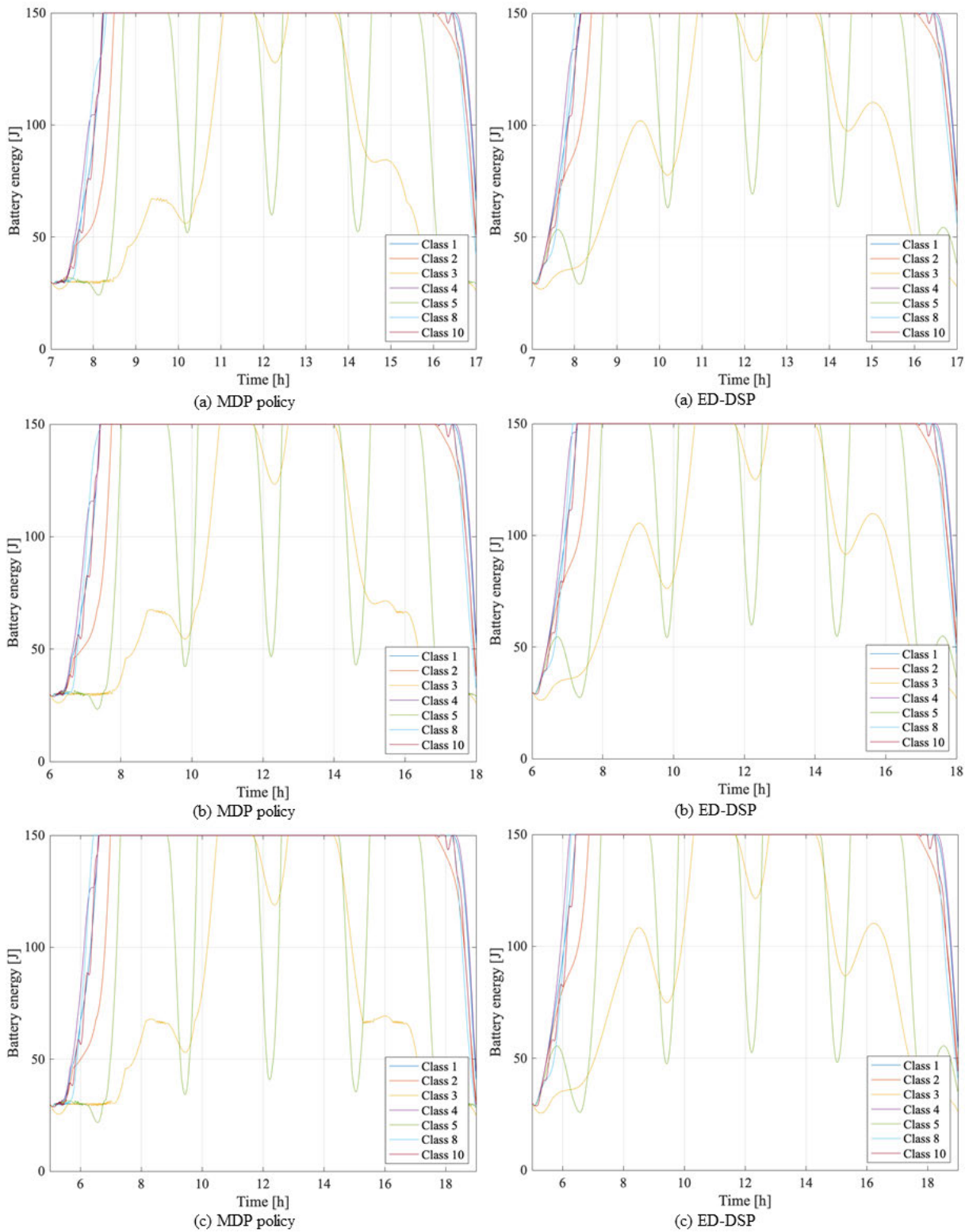
FIGURE 17. Graphs of the battery energy vs time of the MDP policy (left) and ED-DSP (right): (a) 10h (7 AM-5 PM), (b) 12h (6 AM-6 PM), and (c) 14h (5 AM-7 PM).

over the 10,000J, but classes 3 and 5 are very low. Hence, the operations in classes 1, 2, 4, 8, and 10 of the MDP policy

are similar to the ED-DSP. In contrast, in classes 3 and 5, the MDP policy tends to consume more battery energy than
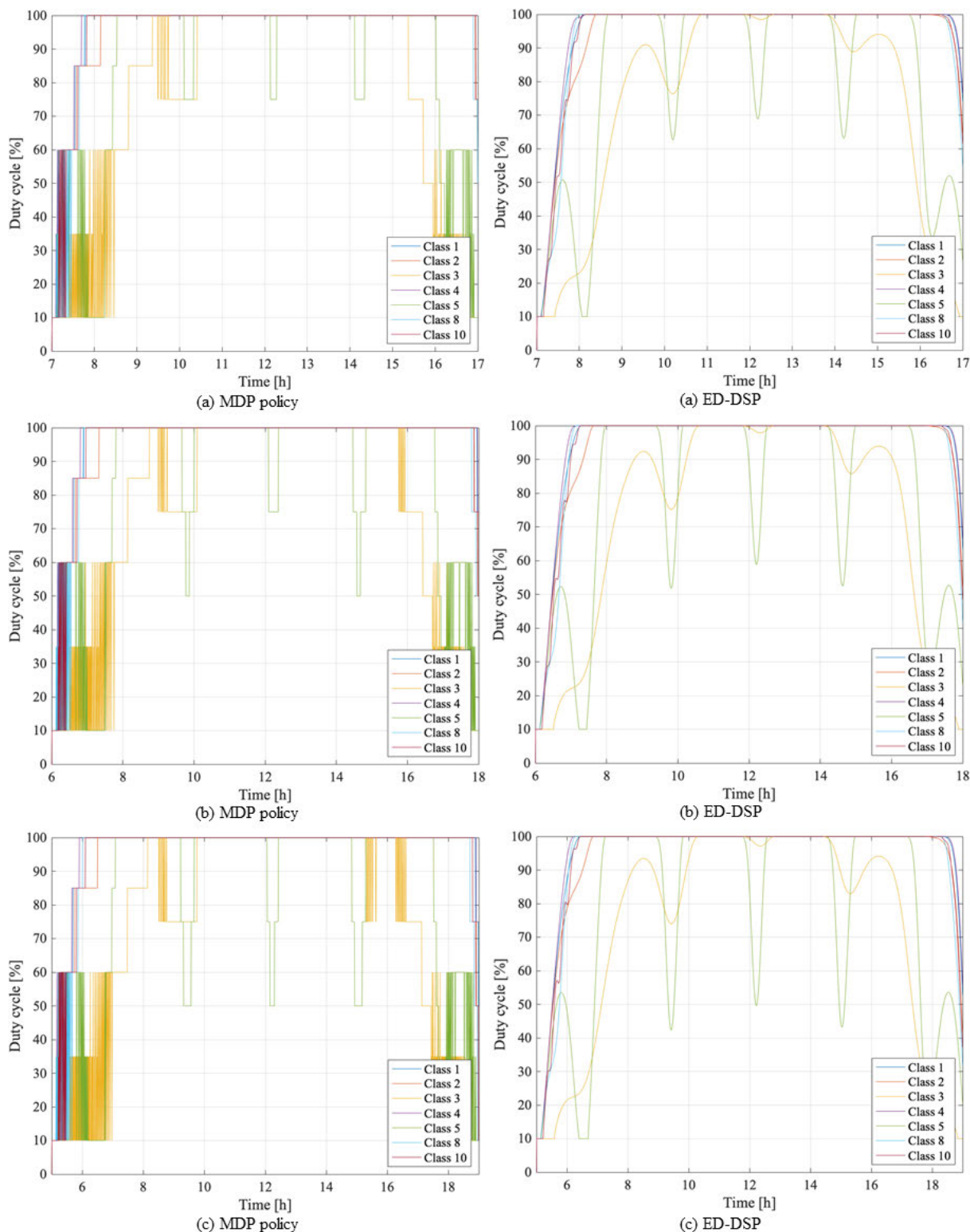
FIGURE 18. Graphs of the duty cycle vs time of the MDP policy (left) and ED-DSP (right): (a) 10h (7 AM-5 PM), (b) 12h (6 AM-6 PM), and (c) 14h (5 AM-7 PM).

the ED-DSP. Consequently, the MDP policy can manage the battery energy under the low solar irradiance better than the ED-DSP.

Fig. 16 illustrates the duty cycle during operations from 6 AM to 6 PM in the different battery capacities. Both MDP and ED-DSP operate with no zero-duty cycle. On the one

TABLE 10. Amounts of the data transfer in the different solar irradiance classes and battery capacities from 6 AM to 6 PM.

Class	Amount of the data transfer [Gbit]								
	50J			150J			500J		
	MDP policy	ED-DSP	Δ	MDP policy	ED-DSP	Δ	MDP policy	ED-DSP	Δ
Class 1	10.2949	10.2619	0.0330	10.4366	10.3150	0.1217	10.2244	10.0764	0.1480
Class 2	10.1779	10.1503	0.0276	10.3436	10.2056	0.1380	10.1273	9.9655	0.1617
Class 3	7.7351	7.7016	0.0335	7.9451	7.8669	0.0783	8.5316	8.1989	0.3327
Class 4	10.3136	10.2897	0.0239	10.4614	10.3491	0.1123	10.2469	10.1086	0.1383
Class 5	7.9980	7.9525	0.0455	8.8492	8.6541	0.1951	9.5730	9.3426	0.2304
Class 8	10.0811	10.0587	0.0224	10.3001	10.1831	0.1170	10.1813	10.0208	0.1605
Class 10	10.1640	10.1357	0.0283	10.3481	10.2270	0.1211	10.1768	10.0324	0.1443

TABLE 11. Amounts of the data transfer in the different solar irradiance classes and period of the daytime with 150J battery capacity.

Class	Amount of the data transfer [Gbit]								
	10h (7 AM-5 PM)			12h (6 AM-6 PM)			14h (5 AM-7 PM)		
	MDP policy	ED-DSP	Δ	MDP policy	ED-DSP	Δ	MDP policy	ED-DSP	Δ
Class 1	8.6992	8.5872	0.1121	10.4366	10.3150	0.1217	12.1695	12.0383	0.1312
Class 2	8.6265	8.4994	0.1271	10.3436	10.2056	0.1380	12.0495	11.9064	0.1431
Class 3	6.6600	6.5857	0.0743	7.9451	7.8669	0.0783	9.2314	9.1470	0.0844
Class 4	8.7191	8.6155	0.1037	10.4614	10.3491	0.1123	12.1991	12.0776	0.1215
Class 5	7.5079	7.3199	0.1880	8.8492	8.6541	0.1951	10.1524	9.9700	0.1824
Class 8	8.6032	8.4941	0.1092	10.3001	10.1831	0.1170	11.9723	11.8651	0.1071
Class 10	8.6385	8.5224	0.1161	10.3481	10.2270	0.1211	12.0450	11.9254	0.1196

hand, the MDP policy discretely changes the duty cycle in a step of 25% due to the number of the duty cycle N equal to 5 levels. On the other hand, the ED-DSP continuously changes the duty cycle following the residual battery energy.

Next, the simulation results of the operation with the battery capacity equal to 150J in the different daytime periods are presented. Fig. 17 illustrates the battery energy of the MDP policy and ED-DSP. Both MDP policy and ED-DSP show that the shorter period of the daytime, the lower battery energy at the end of the day. Even when the period of the day is shrunk or expanded, the MDP policy still manages the battery energy better than the ED-DSP.

Fig. 18 illustrates the duty cycle of the MDP policy and ED-DSP operating in the different daytime periods. Both MDP policy and ED-DSP can transmit data over the daytime because the duty cycle does not reach zero. When the period is short or long, the duty cycle looks similar to each other. However, the longer daytime yields a lower duty cycle and the residual energy at the end of the daytime.

The amounts of the data transfer in the daytime and different battery capacities and period of the daytime are shown in Table 10 and Table 11 respectively. The amounts of data transfer are directly proportional to the potentially charged energy as shown in Table 5. In all cases, the MDP policy can transmit more data than the ED-DSP.

Table 10 shows that the large battery capacity does not always yield the maximum data transfer. In the case of the MDP policy, the suitable size can be calculated by the relation between the energy consumption and battery capacity. For example, this MDP model is generated by $M = 27$ and $N = 5$, and the maximum energy consumption of the MICAz mote and transceiver in the active mode during the 30s is equal to 2.742J. According to Condition 1, the maximum battery in the MDP model equal to

TABLE 12. Amounts of the data transfer in the entire year.

Area/Year	Amount of the data transfer [Gbit]		
	MDP policy	ED-DSP	Δ
Golden, Colorado/2019	2107.0331	2094.9037	12.1294
Eugene, Oregon/2020	2074.1614	2062.8563	11.3051
Milford, Utah/2012	1944.0281	1934.3690	9.6591
Edinburg, Texas/2017	2544.8550	2532.3614	12.4936

(2.742)(27-1)/(5-1) = 17.823J. Then, the threshold battery is 30J, so that the suitable battery capacity should be 47.823J or approximately 50J. Hence, the amounts of the data transfer in the 500J battery capacity are less than the 50J and 150J capacities.

In the case of the ED-DSP, the duty cycle is adjusted by the residual energy. Even if the battery capacity is larger, the duty cycle is still limited to 100%. If the battery capacity is large and the initial battery energy is very low, the duty cycle will gradually increase to 100%. In contrast, if the battery capacity is small and the initial battery energy is very low, the duty cycle will sharply increase to 100%. As the result, the low battery capacity yields more amount of data transfer than the high battery capacity.

Table 11 illustrates the amounts of the data transfer in the different periods of the daytime. the amount of the data transfer is directly proportional to the time, and the MDP policy has a better performance than the ED-DSP.

In Table 10 and 11, all different amounts of data transfer Δ are positive, so that the MDP policy can transfer data more than the ED-DSP in all cases. Therefore, the MDP policy has better performance than the ED-DSP both in the variety of battery capacities and time periods.

C. SIMULATION RESULTS WITH REAL SOLAR IRRADIANCE DATA

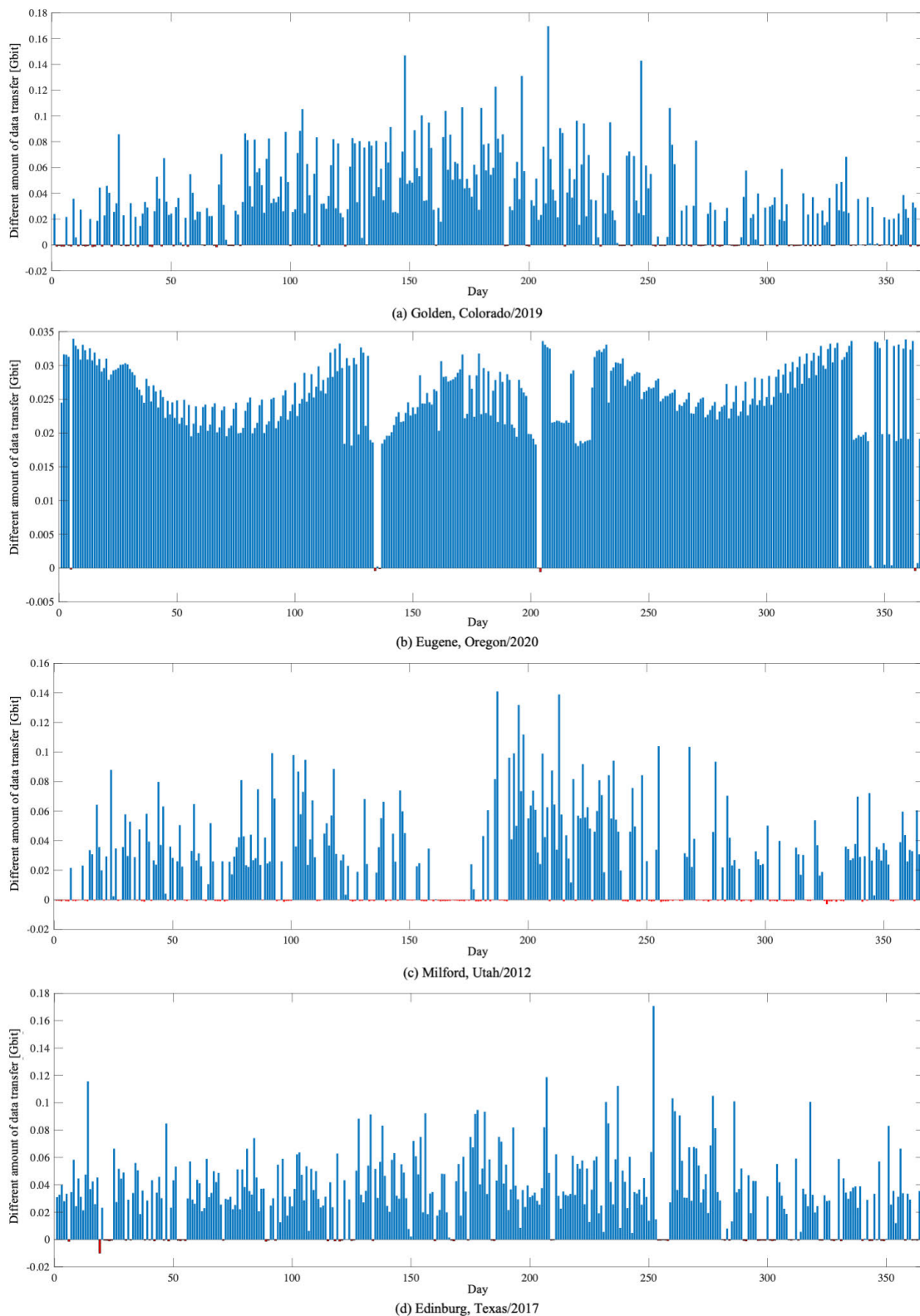Table 12 shows amounts of data transfer for the entire year of the MDP policy and ED-DSP in different areas. The MDP

FIGURE 19. Graphs of the different amounts of data transfer in different areas in the U.S.

policy transfers more data than the ED-DSP for all areas. The results clearly show that the MDP policy has a better performance than the ED-DSP.

Fig. 19 illustrates different amounts of data transfer Δ for a whole year. The positive difference Δ^+ (blue bar) means the amount of data transfer of the MDP policy is higher than

TABLE 13. Average values of the positive and negative different amounts of data transfer, and numbers of the days that MDP policy transfers more data than ED-DSP and vice versa.

Area/Year	Δ_{ave}^+ [Gbit]	Δ_{ave}^- [Gbit]	Number of days	
			MDP >	ED-DSP >
Golden, Colorado/2019	0.0458	-0.0007	261	104
Eugene, Oregon/2020	0.0254	-0.0003	360	6
Milford, Utah/2012	0.0453	-0.0007	203	163
Edinburg, Texas/2017	0.0421	-0.0008	291	74

the ED-DSP, and the negative difference Δ^- (red bar) means the amount of data transfer of the ED-DSP is higher than the MDP policy. Almost all the positive differences are higher than the negative differences.

Table 13 shows average values of the positive and negative different amounts of data transfer (Δ_{ave}^+, Δ_{ave}^-), and also numbers of days that the MDP policy transfers more data than ED-DSP (MDP >) and vice versa (ED-DSP >). The average values of the positive and negative different amounts of data transfer can be calculated from (30) and (31).

$$\Delta_{ave}^+ = \frac{\sum_{g \in \mathscr{G}} \Delta_g}{G} \quad (30)$$

where g is the day that the MDP policy transfers more data than the ED-DSP and G is the number of the days that the MDP policy transfers more data than the ED-DSP.

$$\Delta_{ave}^- = \frac{\sum_{q \in \mathscr{Q}} \Delta_q}{Q} \quad (31)$$

where q is the day that the ED-DSP transfers more data than the MDP policy and Q is the number of the days that the ED-DSP transfers more data than the MDP policy.

The average of the positive difference is over 0.0250Gbits, but the maximum average of negative difference is only 0.0008Gbits. Hence, the MDP policy can transfer data over ED-DSP more than 31.25times (0.0250/0.0008) of the day that the ED-DSP can transfer data over the MDP policy.

The minimum number of days that the MDP policy transfers more data than the ED-DSP is 203days. So that, the MDP policy can transfer data over the ED-DSP at least (203/366) × 100 = 55.46% a year.

Consequently, the MDP policy has a discrete change in the duty cycle and can be operated in different solar irradiance classes. It can transfer more data than the ED-DSP at least 9.6591Gbits a year. Hence, if the cost of the data service equals to 10$ per one Gbit, the MDP policy can gain at least 289$ a year more than the ED-DSP for one node.

VII. CONCLUSION

Solar energy harvesting with PV panels is one viable solution to sustaining the battery energy of WSN nodes. To manage battery energy and data transfer, the MDP can be used to decide when to allow an SEH-WSN node to change its duty cycle, which will allow the node to yield maximum data transfer while maintaining battery energy close to the threshold battery level.

In this article, the communication between the SEH-WSN node and base station is one hop style, where the base station can receive data from others nodes simultaneously. The MDP state is a set that consists of the pair of battery energy and duty cycle of the node. The duty cycle of each node can only be adjusted by one level per decision-making. The reward is determined as the amount of the data transfer. Transition probability matrices are constructed by solar irradiance probability, as calculated from the hourly solar irradiance model. Then, linear programming is used to solve this MDP problem to obtain the optimal policy that will be programmed in the node.

The simulations with the solar irradiance model (Classes 1-5, 8, and 10) show that the MDP policy and the ED-DSP can transfer data throughout the daytime and prevent the depletion of the battery. In addition, the MDP policy transfers more data than the ED-DSP in the different irradiance classes.

The simulations with the annual data from Colorado, Oregon, Utah, and Texas show that the MDP policy can transfer data more than the ED-DSP throughout the year. Most of the days in the year, the MDP policy transfers more data than the ED-DSP. Therefore, The MDP policy outperforms the ED-DSP with the ideal prediction.

For future work, the authors will develop the MDP policy with multi-hop communication. Then, scalability and fairness can be considered.

REFERENCES

[1] M. Ayaz, M. Ammad-Uddin, I. Baig, and E.-H.-M. Aggoune, "Wireless sensor's civil applications, prototypes, and future integration possibilities: A review," *IEEE Sensors J.*, vol. 18, no. 1, pp. 4–30, Jan. 2018.

[2] B. Cheng, S. Zhao, J. Qian, Z. Zhai, and J. Chen, "Lightweight service mashup middleware with REST style architecture for IoT applications," *IEEE Trans. Netw. Service Manage.*, vol. 15, no. 3, pp. 1063–1075, Sep. 2018.

[3] J. Feng and H. Chen, "Repairing confident information coverage holes for big data collection in large-scale heterogeneous wireless sensor networks," *IEEE Access*, vol. 7, pp. 155347–155360, 2019.

[4] J. M. C. Silva, K. A. Bispo, P. Carvalho, and S. R. Lima, "Flexible WSN data gathering through energy-aware adaptive sensing," in *Proc. Int. Conf. Smart Commun. Netw. Technol. (SaCoNeT)*, Oct. 2018, pp. 317–322.

[5] N. K. Dixit and K. J. Rangra, "A survey of energy harvesting technologies," in *Proc. Int. Conf. Innov. Control, Commun. Inf. Syst. (ICICCI)*, Aug. 2017, pp. 1–7.

[6] F. Alfayez, M. Hammoudeh, and A. Abuarqoub, "A survey on MAC protocols for duty-cycled wireless sensor networks," *Procedia Comput. Sci.*, vol. 73, pp. 482–489, Dec. 2015.

[7] J. Varghese and A. L. Jose, "Dynamic duty-cycled MAC for wireless sensor networks with energy harvesters," in *Proc. Int. Conf. Circuits, Commun., Control Comput.*, Nov. 2014, pp. 156–160.

[8] W. Ye, J. Heidemann, and D. Estrin, "An energy-efficient MAC protocol for wireless sensor networks," in *Proc. IEEE 21st Annu. Joint Conf. Comput. Commun. Soc.*, vol. 3, Jun. 2002, pp. 1567–1576.

[9] V. L. Quintero, C. Estevez, M. E. Orchard, and A. Perez, "Improvements of energy-efficient techniques in WSNs: A MAC-protocol approach," *IEEE Commun. Surveys Tuts.*, vol. 21, no. 2, pp. 1188–1208, 2nd Quart., 2019.

[10] A. Kansal, J. Hsu, S. Zahedi, and M. B. Srivastava, "Power management in energy harvesting sensor networks," *ACM Trans. Embedded Comput. Syst.*, vol. 6, no. 4, p. 32, Sep. 2007, doi: 10.1145/1274858.1274870.

[11] J. R. Piorno, C. Bergonzini, D. Atienza, and T. S. Rosing, "Prediction and management in energy harvested wireless sensor nodes," in *Proc. 1st Int. Conf. Wireless Commun., Veh. Technol., Inf. Theory Aerosp. Electron. Syst. Technol.*, May 2009, pp. 6–10.

[12] D. K. Noh and K. Kang, "Balanced energy allocation scheme for a solar-powered sensor system and its effects on network-wide performance," *J. Comput. Syst. Sci.*, vol. 77, no. 5, pp. 917–932, Sep. 2011. [Online]. Available: https://www.sciencedirect.com/science/article/pii/S0022000010001236

[13] A. Cammarano, C. Petrioli, and D. Spenza, "Pro-energy: A novel energy prediction model for solar and wind energy-harvesting wireless sensor networks," in *Proc. IEEE 9th Int. Conf. Mobile Ad-Hoc Sensor Syst. (MASS)*, Oct. 2012, pp. 75–83.

[14] S. Kosunalp, "A new energy prediction algorithm for energy-harvesting wireless sensor networks with Q-learning," *IEEE Access*, vol. 4, pp. 5755–5763, 2016.

[15] H. Ren, J. Guo, L. Sun, and C. Han, "Prediction algorithm based on weather forecast for energy-harvesting wireless sensor networks," in *Proc. 17th IEEE Int. Conf. Trust, Secur. Privacy Comput. Commun./12th IEEE Int. Conf. Big Data Sci. Eng. (TrustCom/BigDataSE)*, Aug. 2018, pp. 1785–1790.

[16] I. Sansa, Z. Boussaada, M. Mazigh, and N. M. Bellaaj, "Solar radiation prediction for a winter day using ARMA model," in *Proc. 6th IEEE Int. Energy Conf. (ENERGYCon)*, Sep. 2020, pp. 326–330.

[17] R.-R. Belu, "Design and analysis of a micro-solar power for wireless sensor networks," in *Proc. 9th Int. Conf. Commun. (COMM)*, Jun. 2012, pp. 275–278.

[18] T. N. I. Hong, M. Drieberg, and B. S. M. Singh, "Simulation and hardware implementation of solar energy harvester for wireless sensor networks," in *Proc. IEEE Conf. Syst., Process Control (ICSPC)*, Dec. 2014, pp. 84–89.

[19] L. J. Chien, M. Drieberg, P. Sebastian, and L. H. Hiung, "A simple solar energy harvester for wireless sensor networks," in *Proc. 6th Int. Conf. Intell. Adv. Syst. (ICIAS)*, Aug. 2016, pp. 1–6.

[20] T. Sung, S. Yoon, and K. Kim, "A mathematical model of hourly solar radiation in varying weather conditions for a dynamic simulation of the solar organic rankine cycle," *Energies*, vol. 8, no. 7, pp. 7058–7069, Jul. 2015.

[21] B. O. Kang and K.-S. Tam, "A new characterization and classification method for daily sky conditions based on ground-based solar irradiance measurement data," *Sol. Energy*, vol. 94, pp. 102–118, Aug. 2013. [Online]. Available: http://www.sciencedirect.com/science/article/pii/S0038092X13001400

[22] M. A. Green, E. D. Dunlop, J. Hohl-Ebinger, M. Yoshita, N. Kopidakis, and A. W. Ho-Baillie, "Solar cell efficiency tables (version 55)," *Prog. Photovolt., Res. Appl.*, vol. 28, no. 1, pp. 3–15, 2019.

[23] P. L. A. K. Piyumal, A. L. A. K. Ranaweera, S. R. D. Kalingamudali, and N. Kularatna, "Improving the energy storage of standalone PV systems while enhancing the charging efficiency using supercapacitors," in *Proc. IEEE Int. Conf. Ind. Technol. (ICIT)*, Feb. 2019, pp. 486–490.

[24] D. Niyato, P. Wang, and D. I. Kim, "Optimal service auction for wireless powered Internet of Things (IoT) device," in *Proc. IEEE Global Commun. Conf. (GLOBECOM)*, Dec. 2014, pp. 1–6.

[25] C. Tang, X. Chen, Y. Chen, and Z. Li, "A MDP-based network selection scheme in 5G ultra-dense network," in *Proc. IEEE 24th Int. Conf. Parallel Distrib. Syst. (ICPADS)*, Dec. 2018, pp. 823–830.

[26] K. Woradit and G. Srirutchataboon, "Uplink wireless powered communications of rate-adaptive IoT nodes with intermittent energy source," in *Proc. 16th Int. Conf. Electr. Eng./Electron., Comput., Telecommun. Inf. Technol. (ECTI-CON)*, Jul. 2019, pp. 685–688.

[27] K. Khan and W. Goodridge, "S-MDP: Streaming with Markov decision processes," *IEEE Trans. Multimedia*, vol. 21, no. 8, pp. 2012–2025, Aug. 2019.

[28] D. Bello and G. Riano, "Linear programming solvers for Markov decision processes," in *Proc. IEEE Syst. Inf. Eng. Design Symp.*, Apr. 2006, pp. 90–95.

KANOK CHAROENCHAIPRAKIT (Member, IEEE) received the B.Eng. degree in electrical engineering from the Chulachomklao Royal Military Academy, Thailand, in 2007, and the M.S. degree in electrical engineering from the University of New Haven, CT, USA, in 2011. He is currently pursuing the Ph.D. degree in electrical engineering with Srinakharinwirot University, Thailand. From 2008 to 2009, he was a Signal Maintenance Officer with Royal Thai Army. In 2012, he worked as a Radio Officer. Subsequently, he has been a Lecturer in electrical engineering with the Chulachomklao Royal Military Academy, since 2014. His research interests include digital signal processing, communication systems, and optimization.

WEKIN PIYARAT (Member, IEEE) received the B.Eng. degree in electrical engineering from South-East Asia University, Bangkok, Thailand, in 1994, and the M.Eng. and D.Eng. degrees in electrical engineering from King the Mongkut's Institute of Technology Ladkrabang, Thailand, in 1998 and 2010, respectively. He is currently an Associate Professor with Srinakharinwirot University, Thailand. His research interests include power electronic, electric drives, and control system application.

KAMPOL WORADIT (Member, IEEE) received the B.Eng. (Hons.) and Ph.D. degrees in electrical engineering from Chulalongkorn University, Thailand, in 2002 and 2010, respectively. From 2007 to 2008, he was a Visiting Student with the Laboratory for Information and Decision Systems, Massachusetts Institute of Technology (MIT), MA, USA. He was a Postgraduate Researcher with the Modulation and Coding Department, Institute for Infocomm Research, Singapore. He was a Faculty Member with the Department of Electrical Engineering, Srinakharinwirot University, Thailand, from 2010 to 2020. He is currently a Faculty Member with the Department of Computer Engineering, Chiang Mai University, Thailand. His research interests include wireless communications, the Internet of Things (IoT), and physical layer security. He received the ECTI-CON Best Paper Award, in 2019, and the Royal Golden Jubilee Scholarship from the Thailand Research Fund for his Ph.D. Program.

● ● ●